Table I. Urinary protein excretion and renal function.

	Ctrl	GN+vehicle	GN+TM	GN+CLO
Urinary protein day -1 (mg/dL)	23.0 ± 0.0	23.0 ± 0.0	23.0 ± 0.0	26.0 ± 18.8
day 1 (mg/dL)	32.0 ± 17.6	88.3 ± 11.7	72.0 ± 17.1	88.0 ± 42.7
day 3 (mg/dL)	29.0 ± 18.6	151.7 ± 25.2 †	100.0 ± 0.0 *	160.0 ± 36.7
day 5 (mg/dL)	12.0 ± 5.6	183.3 ± 44.1 †	116.0 ± 36.1 *	206.0 ± 44.0
Body Weight (g)	281.6 ± 2.7	278.7 ± 2.5	280.2 ± 5.6	267.8 ± 3.7
BUN (mg/dL)	17.2 ± 0.9	23.4 ± 3.5	17.1 ± 0.7	28.74 ± 5.5
Creatinine (mg/dL9	0.27 ± 0.03	0.18 ± 0.03	0.26 ± 0.02	0.52 ± 0.13

Body weight at day6. BUN; blood urea nitrogen. Creatinine; serum creatinine. Values are given as the mean ± s.e.m.

Table II. Sequences of primers used for the qRT-PCR (5' to 3')

Gene	Sense primer	Antisense primer
Human Serpine 1	GATGGCTCAGACCAACAAGTTCAA	TGGTAGGGCAGTTCCAGGATG
Human Cd11b	ATAGTGACATTGCCTTCTTG	ATCTTGGGTTAGGGTTGTTC
Human Cd68	AGTGGACATTCTCGGCTCAG	ATGATGAGAGGCAGCAAGAT
Human F4/80	TCGGACGGAATACTTAGACA	TCAGAGGTGGTCAAGGGAGC
Human Tnf	CTCCAGGCGGTGCTTGTTCC	GGCTTGTCACTCGGGGTTCG
Human Il6	CACAGACAGCCACTCACCTC	TCCAAAAGACCAGTGATGAT
Human Csf1r	CATCCTCAGCACCAACAACG	GATAGTCCTGGCTCTGAATG
Human Ccl2	CCTTCTGTGCCTGCTGCTCA	ACTTGCTGCTGGTGATTCTT
Human Lrp	GGGCTCTGGTGGTGGATGTG	AATGTAGTCCTCGCGGGCGT
Human Actb	TGGCACCCAGCACAATGAA	CTAAGTCATAGTCCGCCTAGAAGCA
Rat CD68	AAACAGGACCGACATCAGAG	ATTGCTGGAGAAAGAACTAT
Rat Cd11b	GACATCCCTTCCTTCAACAG	GATGAGAGCCAAGAGCACCA
Rat Actb	GGAGATTACTGCCCTGGCTCCTA	GACTCATCGTACTCCTGCTTGCTG

Materials and Methods

Animals. The studies were performed in 8-week-old C57Bl6/J Jcl female mice and 6-week-old male Sprague-Dawley rats obtained from SLC (Shizuoka Japan). 8-week-old female Balb/c nude mice were obtained from CLEA Japan (Tokyo, Japan). Mice and rats were housed under a 12hr light-dark cycle and given regular chow, MF (Oriental Yeast Co., Ltd.). Homozygous PAI-1 deficient mice and their littermate (wild-type) mice were previously described[1]. All animal experiments conformed to the National Health Guide for the Care and Use of Laboratory Animals and were approved by the Animal Committee at Tohoku University.

Materials. PMA was obtained from Sigma-Aldrich (St. Louis, MO, USA). Dimethyl sulfoxide (DMSO) was purchased from Nacalai Tesque (Kyoto, Japan). Recombinant human PAI-1 and RAP was obtained from Millipore (MA, USA). Recombinant human mutant PAI-1 (Q123K, R76E, T333R) and Alexa fluor -labelled PAI-1 were obtained from Molecular Innovations (MI, USA). Human recombinants LRP1 cluster II and cluster IV were obtained from R&D systems (MN, USA). All other materials were from standard sources and of the highest purity available commercially. The media containing recombinant PAI-1 were investigated by a kit (Toxicolor® system, Seikagaku Corp., Tokyo, Japan) detecting endotoxin levels; they were endotoxin-free (<0.01 EU/ml of endotoxin).

Cell culture conditions. The human monocytic cell line THP-1 was cultured in RPMI 1640 (GIBCO, Paisley, UK) supplemented with 10 % heat-inactivated fetal bovine serum (FBS) (Sigma-Aldrich) under 5 % CO_2.

PAI-1 inhibitor. The recently described PAI-1 inhibitor TM5275, 5-chloro-2-((2-(4-(diphenylmethyl) piperazin-1-yl)-2-oxoethoxy acetyl)amino)benzoate,

was used. TM5275 inhibits the PAI-1 activity with a half-maximal inhibition (IC50) value of 6.95 mM, as measured by assay of tPA-dependent hydrolysis of a peptide substrate. In vitro, TM5275 (up to 100 mM) does not interfere with other serpin/serine protease systems such as alpha1-antitrypsin/trypsin and alpha2-antiplasmin/plasmin. Therefore, its PAI-1–inhibitory activity appears to be specific. Preincubation of PAI-1 with TM5275 abolishes detection of the covalent PAI-1–tPA complex by SDS-PAGE[2]. TM5275 (50 mg/kg), given by gavage in rats, yields calculated plasma T_{max}, C_{max}, and $T_{1/2}$ of 2 h, 34 μmol/L, and 2.5 hr, respectively[2].

In vivo Mf migration assay. The PAI-1 inhibitor TM5275 was resuspended in 200 mL of 0.5% carboxymethylcellulose (MP Biomedicals) and administered orally (10 or 100 mg/kg body weight) daily to mice from day -1 to 4 after thioglycollate broth (BD, Sparks, MD) injection. Mice were injected *i.p.* with 1 mL of 5% sterile thioglycollate broth at day 0. After 4 days, the Mf numbers in the peritoneal lavage were determined by hemocytometer. Giemsa staining confirmed that Mf represented >90% of the cells harvested 4 days after thioglycollate broth injection. Control mice received vehicle only (200 mL of 0.5% carboxymethylcellulose).

In vitro Mf migration assay. Chemotaxis assays were performed as previously described[3], with a modified Boyden chamber. Briefly, THP-1 cells were treated with PMA for 2 days. Cells were collected with 0.05 % Trypsin-EDTA and washed with RPMI1640 medium. ~30,000 cells were pre-incubated with the molecules to be tested at 37 °C for 30 min, and added to the upper well of Boyden chambers (Corning Inc, Corning, NY). Cells were then incubated with the indicated amounts of PAI-1 in the RPMI1640 medium for 24 h at 37 °C. The filters were washed, and the contents of the upper surface of the inserts were removed by cotton swabs. The invading cells at the

bottom surface of the inserts were stained with DiffQuick (Sysmex Corporation, Kobe, Japan) and counted in four random high power fields/insert.

Cytokine analysis Before stimulation, THP-1 cells were differentiated for 48 h in the presence of 50 ng/ml PMA, washed three times, and rested overnight. THP-1 cells (1.5×10^5/well) were incubated with 10 mM of TM5275 or DMSO only for 30 min before stimulation with P. gingivalis or E. coli LPS (100 ng/ml, Wako Pure Chemical Industries, Osaka, Japan) or P. gingivalis or E. coli LPS (100 ng/ml) and IFN-g (20 ng/ml, PeproTech, Rocky Hill, NJ) for 48 hr. Cytokine levels were quantitated using Griess reagent (Sigma-Aldrich, St. Louis, MO, USA) and hIL-6 ELISA Ready-Set-Go kit (eBiosciences, San. Diego, CA, USA), according to the protocol suggested by the manufacturer.

Immunoblot analysis. Immunoblot analysis were performed as described previously[4-6]. Anti-LRP1 (Fitzgerald Industries, International; Action, MA) and anti-b-actin (Sigma-Aldrich) antibodies were used as the primary antibody.

Gene expression analysis. Total RNA was extracted from tissue or cells using ISOGEN (Nippon Gene). Quantitative reverse transcription polymerase-chain reaction (RT-PCR) analysis were performed as described previously[6]. The sequences of the primers are shown in Table S1. Real time RT-PCR was performed on a LightCycler rapid thermal cycler system using a LightCycler 480 SYBR Green I Master (Roche Applied Science) according to the manufacturer's instructions. Data were analyzed by using the comparative Ct method as means of relative quantification, normalized to an endogenous reference (b-actin, Actb) and relative to a calibrator (normalized Ct value obtained from control mice) and expressed as 2^{-DDCt}.

Rat anti-Thy-1 glomerulonephritis model. Glomerulonephritis (GN) was induced by intravenously injection of the monoclonal anti-thy1.1 antibody ER4G (1.0 mg/kg body weight) on day 0. GN rats were divided into 4 groups (n=5-6) as follows: administration of PAI-1 inhibitor, TM5275 (30mg/kg/day), was given orally during the whole observation period (from day -2 to day 7; GN+TM) or clopidogrel (30 mg/kg/day, given during the whole observation period; GN+CLO) or only 0.5% CMC which is vehicle of the drugs every day (GN+vehicle). As a normal control, another group of 5 rats received the same volume of PBS intravenously at Day 0 and orally 0.5% CMC during the whole observation period (control). Urinary excretion of protein was measured with dipstick (Terumo Co., Tokyo, Japan) at day -1, 1, 3 and 5. All rats were anesthetized and blood sample was drawn from the lower abdominal aorta 7 days after the induction of GN. After perfusion with saline, the kidneys were collected.

Histology. Part of the kidneys from individual rats was immersed and fixed overnight in 10% neutral-buffered formalin. Three-micrometer sections of paraffin-embedded tissue were stained with masson trichrome (MT) for aneurysm and collagen scoring, with periodic acid-Schiff (PAS) for matrix expansion, with phosphotungstic acid hematoxylin (PTAH) for fibrin deposition, and with hematoxylin-eosin (HE). The area of microaneurysm occupying each glomerulus and glomerular sclerosis[7] were scored as 1 (0-25%), 2 (25-50%), 3 (50-75%), or 4 (75-100%) as shown in Fig. 6A-D, respectively. The area of mesangial matrix and fibrin deposition occupying each glomerulus was assessed by ImageJ™ software (version 1.440, National Institute of Health, Bethesda, MD, USA). The number of nuclei per glomerular cross section was counted in 50 glomeruli and averaged. All microscopic examinations were performed in 50 randomly selected glomeruli from each rat by two independent observers in blinded manner.

Immunohistochemistry Indirect immunoperoxidase staining with an anti-CD68 monoclonal antibody was used to detect monocytes and Mf (1:400, ED1; Abd Serotec, Kidlington, Oxford, UK). Briefly, sections were autoclaved in 0.01 M citrate buffer (pH 6.0) at 120 °C for 5 min or were trypsinized with 0.1% trypsin, 0.1% CaCl2, in 0.05 M Tris buffer (pH 7.6) at 37 °C for 10min in order to retrieve antigen, or were digested with Proteinase K (Proteinase K Ready-to-use; Dako, Glostrup, Denmark) in order to improve the accessibility of antigen, and then immersed in 50% methanol containing 0.3% H_2O_2 to quench endogenous peroxidase activity. Signals were amplified with the immunohistochemical staining system (Histofine simple stain MAX-PO; Nichirei Bioscience Inc., Tokyo, Japan or EnVision^{TM}+Mouse/HRP; DAKO Co.), visualized by DAB, and counterstained with hematoxylin.

In each slide, the number of ED1-positive cells was assessed in glomeruli. Positive areas of desmin in glomeruli were evaluated by ImageJ^{TM} software. All microscopic examinations were performed in 50 randomly selected glomeruli from each rat by two independent observers in blinded manner.

Effect of TM5275 on direct binding between PAI-1 and LRP1 Cluster II, or Cluster IV. Direct binding analysis was performed as previously described[8]. Briefly, 100 ng of LRP, cluster II, or cluster IV was immobilized for 16 h at 4 °C in microtiter wells in 50 mM NaHCO3 (pH 8.6) in a volume of 50 ml. Subsequently, wells were blocked for 1 h at 37 °C with 3% (w/v) BSA in modified HBST buffer in a volume of 300 ml, washed with modified HBST buffer. The wells were then washed and incubated for 1 h at 37 °C in modified HBST buffer with Alexa fluor 488-labelled PAI-1, with or without pre-treatment of 10 mM TM5275 for 30 min at 37 °C. Bound proteins were measured using the SpectraMax Gemini XS (Molecular Devices, Inc., Sunnyvale, CA) as fluorescent intensity. The data were analyzed with Softmax software, and each data

point presented was the average of a triplicate determination. As controls, direct Alexa-488 labelled PAI-1 binding to immobilized BSA was measured.

ELISA. Blood was collected into tubes containing 0.1 volume of 3.8% sodium citrate for plasma, or tubes containing gel/clot activator (VENOJECT II, Terumo Co., Tokyo, Japan) for serum. Plasma levels of active PAI-1 were measured using the ELISA kit (Molecular Innovations). Serum levels of creatinine and BUN were measured with FUJI DRY-CHEM 3500 (FUJIFILM Co., Tokyo, Japan).

Statistical analysis. The level of significance for the difference between data sets was assessed using the Student's t-test. Analysis of variance followed by Tukey's test was used for multiple comparisons. Proteinuria excretion and microaneurysm severity were analyzed by two-way analysis of variance. Differences between multiple groups were analyzed by one-way analysis of variance or Kruskal-Wallis test in the case of a non-Gaussian distribution, followed by the Bonferroni, Dunn's or Tukey's post-hoc test for comparison between treatment groups. All statistical analyses were performed using the Prism software (version 5.0, GraphPad Software, La Jolla, CA, USA). Data were expressed as means $\pm$ standard error. $P<0.05$ was considered to be statistically significant.

1. Carmeliet P, Kieckens L, Schoonjans L, Ream B, van Nuffelen A, Prendergast G, Cole M, Bronson R, Collen D, Mulligan RC. Plasminogen activator inhibitor-1 gene-deficient mice. I. Generation by homologous recombination and characterization. *J Clin Invest*. 1993;92:2746-2755.
2. Izuhara Y, Yamaoka N, Kodama H, Dan T, Takizawa S, Hirayama N, Meguro K, van Ypersele de Strihou C, Miyata T. A novel inhibitor of plasminogen activator inhibitor-1 provides antithrombotic benefits devoid of bleeding effect in nonhuman primates. *J Cereb Blood Flow Metab*. 2010;30:904-912.

3. Degryse B, Neels JG, Czekay RP, Aertgeerts K, Kamikubo Y, Loskutoff DJ. The low density lipoprotein receptor-related protein is a motogenic receptor for plasminogen activator inhibitor-1. *J Biol Chem.* 2004;279:22595-22604.

4. Ichimura A, Hirasawa A, Poulain-Godefroy O, *et al.* Dysfunction of lipid sensor GPR120 leads to obesity in both mouse and human. *Nature.* 2012;483:350-354.

5. Hirasawa A, Tsumaya K, Awaji T, Katsuma S, Adachi T, Yamada M, Sugimoto Y, Miyazaki S, Tsujimoto G. Free fatty acids regulate gut incretin glucagon-like peptide-1 secretion through GPR120. *Nat Med.* 2005;11:90-94.

6. Ichimura A, Ruike Y, Terasawa K, Shimizu K, Tsujimoto G. MicroRNA-34a inhibits cell proliferation by repressing mitogen-activated protein kinase kinase 1 during megakaryocytic differentiation of K562 cells. *Mol Pharmacol.* 2010;77:1016-1024.

7. Raij L, Azar S, Keane W. Mesangial immune injury, hypertension, and progressive glomerular damage in Dahl rats. *Kidney Int.* 1984;26:137-143.

8. Neels JG, van Den Berg BM, Lookene A, Olivecrona G, Pannekoek H, van Zonneveld AJ. The second and fourth cluster of class A cysteine-rich repeats of the low density lipoprotein receptor-related protein share ligand-binding properties. *J Biol Chem.* 1999;274:31305-31311.

e-Blood

In vivo imaging visualizes discoid platelet aggregations without endothelium disruption and implicates contribution of inflammatory cytokine and integrin signaling

Satoshi Nishimura,[1,2] Ichiro Manabe,[1-3] Mika Nagasaki,[1,4] Shigeru Kakuta,[5,6] Yoichiro Iwakura,[5,7] Naoya Takayama,[8] Jun Ooehara,[8] Makoto Otsu,[8] Akihide Kamiya,[8] Brian G. Petrich,[9] Tetsumei Urano,[10] Takafumi Kadono,[11] Shinichi Sato,[11] Atsu Aiba,[12] Hiroshi Yamashita,[1] Seiryo Sugiura,[13] Takashi Kadowaki,[2,3,14] Hiromitsu Nakauchi,[8] Koji Eto,[8,15] and Ryozo Nagai[1-3]

[1]Department of Cardiovascular Medicine, [2]Translational Systems Biology and Medicine Initiative, [3]Global COE Program, Comprehensive Center of Education and Research for Chemical Biology of the Diseases, [4]Computational Diagnostic Radiology and Preventive Medicine, and [5]Laboratory of Molecular Pathogenesis, Center for Experimental Medicine and Systems Biology, University of Tokyo, Tokyo, Japan; [6]Division of Laboratory Animal Research, Research Center for Human and Environmental Sciences, Shinshu University, Nagano, Japan; [7]Core Research for Evolutional Science & Technology (CREST), Japan Science and Technology Agency, Tokyo, Japan; [8]Division of Stem Cell Therapy and Stem Cell Bank, Center for Stem Cell Biology and Regenerative Medicine, Institute of Medical Science, University of Tokyo, Tokyo, Japan; [9]Department of Medicine, University of California–San Diego, La Jolla, CA; [10]Department of Physiology, Hamamatsu Medical University, Hamamatsu, Japan; [11]Department of Dermatology, [12]Laboratory of Animal Resources, Center for Disease Biology and Integrative Medicine, Faculty of Medicine, [13]Department of Human and Engineered Environmental Studies, Graduate School of Frontier Sciences, and [14]Department of Metabolic Diseases, University of Tokyo, Tokyo, Japan; and [15]Center for iPS Cell Research and Application, Kyoto University, Kyoto, Japan

The mechanism by which thrombotic vessel occlusion occurs independently of plaque development or endothelial cell (EC) disruption remains unclear, largely because of an inability to visualize the formation of thrombus, especially at the single-platelet level in real time. Here we demonstrate that rapidly developing thrombi composed of discoid platelets can be induced in the mesenteric capillaries, arterioles, and large-sized arteries of living mice, enabling characterization of the kinetics of thrombosis initiation and the multicellular interrelationships during thrombus development. Platelet aggregation without EC disruption was triggered by reactive oxygen species (ROS) photochemically induced by moderate power laser irradiation. The inflammatory cytokines TNF-α and IL-1 could be key components of the EC response, acting through regulation of VWF mobilization to the cell surface. Thrombus formation was then initiated by the binding of platelet GPIbα to endothelial VWF in our model, and this effect was inhibited by the ROS scavenger N-acetylcysteine. Actin linker talin-dependent activation of alphaIIb-beta3 integrin or Rac1 in platelets was required for late-phase thrombus stability. Our novel imaging technology illustrates the molecular mechanism underlying inflammation-based thrombus formation by discoid platelets on undisrupted ECs and suggests control of ROS could be a useful therapeutic target for the prevention of thrombotic diseases. (*Blood*. 2012;119(8): e45-e56)

Introduction

It is evident that inflammation plays a central role in the pathogenesis of cerebral and cardiovascular diseases, and the thrombotic response is an integral part of these inflammatory processes. Proinflammatory cytokines such as TNF-α and IL-1 promote coagulation with increased tissue factor expression,[1] which in turn induces synthesis of pro–IL-1β in platelets.[2] However, the cytokine-related, multicellular kinetics at the single-platelet level during the development of thrombus in vivo remain unclear because of the absence of a real-time visualization technique with sufficient resolution to assess single-platelet kinetics in living animals.

FeCl₃-induced thrombus formation in carotid arteries is a frequently used model, but it takes minutes to completely occlude the affected vessel.[3,4] Moreover, this method does not allow one to track single-platelet kinetics during the formation of thrombus. Jackson et al succeeded in following a single discoid platelet in a developing thrombus and suggested activated platelets mediate the formation of thrombus via shape changes under low shear conditions, whereas discoid platelets are incorporated into growing thrombi only under high shear conditions.[5,6] However, the precise mechanisms are unknown. In addition, conventional thrombosis models appear to involve endothelial cell (EC) disruption and exposure of the subendothelial matrix.

However, it is now clinically evident that platelet aggregation can occur on undisrupted endothelium within atherosclerotic lesions,[7] making it important for us to learn how thrombus formation occurs on undisrupted and structurally intact endothelium. We therefore developed a novel in vivo imaging method that enables clear visualization of single platelet kinetics within aggregations of discoid platelets in a thrombus developing on undisrupted endothelium. It also enables clarification of the respective

This article contains a data supplement.

contributions made by inflammatory cytokines, integrin activation, and actin reorganization to thrombus formation.

Reactive oxygen species (ROS) are thought to play major roles in the development of atherosclerosis and thrombosis.[8] ROS cause EC dysfunction, contributing to thrombus formation in vivo,[9] but the precise relationship between ROS and inflammatory cytokines during thrombosis is not yet clear. To address that issue, we recently developed an in vivo animal model of thrombosis.[10] and although we suggested that moderately increased ROS levels induced by a photochemical reaction could quickly lead to vessel occlusion, the mechanism was not defined. Since then, we have optimized our technology, and here we show that our in vivo laser injury system induces rapid formation of thrombi composed of discoid platelets without apparent EC disruption.

VWF is a glycoprotein produced in ECs and megakaryocytes and is also present in the extracellular matrix, circulating plasma, and platelets.[11] VWF contributes to the adhesion and aggregation of platelets in disrupted vessels and is critical for hemostasis and thrombosis. VWF is stored inside the Weibel-Palade bodies and undergoes exocytosis after stimulation of ECs by ROS, especially O_2^-.[12,13] We visualized the mobilization of VWF to the EC surface in laser/ROS-stimulated vessels and demonstrated that the binding of platelet GPIbα to VWF on the endothelial surface is the first step in the formation of thrombus. Platelet attachment to undisrupted endothelium was followed by actin-dependent thrombus stabilization mediated by actin-linker talin-dependent activation of integrin[14,15] and Rac1, a small Rho family GTPase.[16,17] Herein we found that inflammatory cytokines contribute to the mobilization of VWF, leading to the platelet aggregations. Jackson et al's findings[5,6] that shear gradient induced the discoid platelet aggregations might be related to our findings, but they did not claim the specific molecular mechanisms. Thus, it is tempting to speculate that shear gradient changes and inflammatory cytokine signaling coordinately contribute to the discoid platelet aggregations leading to the vessel occlusion.

Methods

An expanded methods section is available in supplemental Methods (see the Supplemental Materials link at the top of the article).

Cells, reagents, and mice

Male C57BL/6J mice, age-matched integrin mutant mice (L746A and Y747A knock-in mice), TNF-α knockout (KO), TNF-α–R1 KO, IL-1 α/β double KO, and IL-1RA KO mice were used.[15,18-21] Platelet-specific Rac1 KO mice (Pf4-Rac1 KO) were generated by mating Rac1 flox/flox mice and Pf4-Cre transgenic mice that were kindly provided from Dr Radek Skoda (University Hospital Basel).[22,23] To obtain chimeric mice, BM cells from wild-type, TNF-α KO, or TNF-R1 KO mice were intravenously transfused into lethally irradiated recipient mice. All animals and recombinant DNA experiments were approved by the Institutional Animal Care and Use Committee and strictly followed the guidelines for animal experiments of The University of Tokyo.

Intravital microscopy and formation of thrombus

To visually analyze thrombus formation in the microcirculation of the mesentery in living animals, we used in vivo laser/ROS injury with a visualization technique developed through the modification of conventional methods.[10,24] Anesthetized mice with a small incision made so that the mesentery could be observed without being exteriorized were administrated FITC-dextran (molecular weight [MW] 150 kDa and 10 kDa) or Texas-Red–dextran (MW 70 kDa), and hematoporphyrin (1.8 mg/kg in capillaries and

5 mg/kg in arterioles and arteries) was injected to produce ROS on laser irradiation. Blood cell dynamics and thrombus formation were visualized during laser excitation, and ROS production (wave length 488 nm, 1.5 mW power at 100× objective lens). Sequential images were obtained with a spinning-disk confocal microscope (CSU-X1; Yokogawa) or a Nikon A1R System with a resonance scanning system.

Image analysis

To quantify platelet dynamics, sequential images (covering > 20 seconds) were obtained and analyzed as follows. To assess the initial adherence of the platelets, attachment was defined as continuous interaction (for > 2 seconds) with the endothelium by a platelet after laser-induced injury. It was quantified as the adherent platelet numbers per observed vascular length (usually 100 μm) per observation period). To quantify the development of thrombus, platelet numbers within thrombi were determined as the number of platelets tightly sticking to a vessel (> 2 seconds) or stabilized within the vessel (not moved by blood flow > 2 seconds) per observed vascular length (usually 100 μm) at 10 seconds and 20 seconds after laser injury.

FACS analysis of washed mouse platelets and HUVECs

Washed mouse platelets from wild-type C57BL/6J, TNF-α KO, and TNF-R1 KO mice and cultured HUVECs were stimulated with the use of hematoporphyrin (as a source of O_2^- by laser irradiation), H_2O_2, and/or N-acetylcysteine (NAC). Some HUVECs were also treated with si-RNA targeting TNF-receptor-1 (si-TNF-R1) or with control scrambled si-RNA (si-CTRL) 48 hours before the experiments.

Statistics

We expressed the results as means ± SEM. The statistical significance of differences between 2 groups was assessed by the use of Student t tests. Differences between more than 2 groups were evaluated with ANOVA followed by posthoc Bonferroni tests. We examined correlations by using the Pearson correlation coefficient test. Values of $P < .05$ were considered significant.

Results

Photochemically generated ROS induce thrombi composed of discoid platelets without apparent EC disruption

To induce thrombus formation, we optimized a visualization system in which ROS are produced through a photochemical reaction within mesenteric capillaries.[10] Our improved multicolor in vivo imaging technique enabled clear visualization of the real-time kinetics of leukocytes (Hoechst+), single platelets (anti-GPIbβ), and erythrocytes (fluorescent dextran; Figure 1A and supplemental Video 1). The conventional laser-induced thrombosis method uses a high-power laser to irradiate a limited area of endothelial surface, which disrupts the endothelium and exposes the collagen layer.[3] In our model, by contrast, ROS (specifically O_2^-)[25,26] are produced from hematoporphyrin by the use of moderate-power laser irradiation of the entire imaging field. By using this approach, we were able to induce thrombus formation on undisrupted endothelium (Figure 1B and supplemental Video 2). Thereafter, we sought to clarify how aggregates of discoid platelets form on the undisrupted endothelium in response to ROS.

After laser irradiation, platelets immediately started attaching to the vessel wall, after which they piled up, retarding blood flow, and the vessel lumen was eventually occluded by erythrocytes and/or leukocytes that formed a plug. The reproducibility of this system was confirmed by the finding that 90.5% ± 2.4% (n = 50 vessels from 5 animals) of the blood vessels tested were occluded. Two of
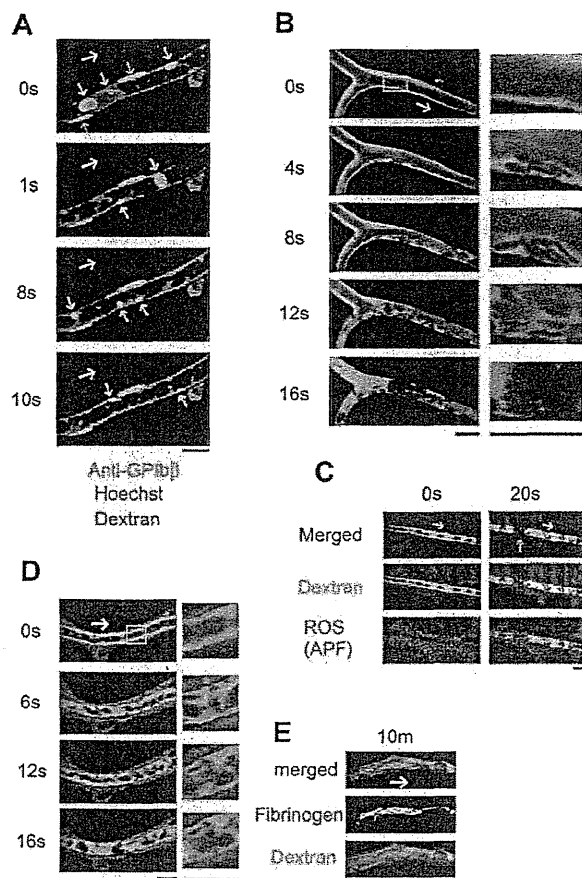
Figure 1. Thrombus formed by discoid platelets visualized by in vivo imaging after laser/ROS-induced injury. (A) In vivo imaging enabling selective visualization of multiple cell types. Platelets, erythrocytes, and leukocyte/EC nuclei were visualized with an anti-GPIbβ antibody (green), fluorescent dextran (red), and Hoechst 33 342 (blue), respectively, in mesenteric capillaries of 12-week-old male control mice. Correspondingly colored arrows point to each cell type, and the white arrow indicates the direction of blood flow. (B) Discoid platelets contribute to thrombus formation after laser/ROS-induced injury. The microcirculation of the mesentery in living animals was visualized after laser/ROS-induced initiation of thrombus formation. (C) ROS production triggers thrombus formation. ROS production in the affected blood vessel after laser/ROS-induced injury was visualized by the administration of APF (red) with dextran (green). The red arrow indicates the developing thrombus. Original movies for panels A and B are available as supplemental Videos 1 and 2. (D-E) Distrbution of fibrinogen in a developing thrombus after short-term (D, 0-20 seconds) and long-term (E, 10 minutes) laser-induced injury. Injected fluorescent fibrinogen is shown in red, and dextran is in green. All scale bars are 10 μm.

the most striking findings were that the platelets retained a discoid shape within the developing thrombi and that the platelets attached to the apparently undisrupted endothelial wall, not to the exposed extracellular matrix. Laser/ROS-induced injury did not cause apparent disruption in the endothelium (supplemental Figure 1). We were also able to induce thrombus formation in small mesenteric arterioles (diameters, 30.5 ± 2.4 μm; n = 20) with almost 100% reproducibility by increasing the concentration of hematoporphyrin and the duration of laser irradiation (1 minute). Single platelets also could be visualized in the arterioles (Figure 2A).

To better define the cell population within the thrombi, we repeated the thrombosis protocol in the presence of a fluorescent anti-GPIbβ antibody to selectively identify platelets. We observed that platelets comprised almost 90% of the cells within the thrombi in both the capillaries and arterioles (supplemental Figure 2), that is these thrombi were composed mainly of discoid platelets and were largely devoid of other cell types, such as leukocytes and/or

erythrocytes. This finding is in stark contrast to FeCl$_3$-induced thrombi, which are composed of several other cell types.[4] In our model, moreover, vessel occlusion was quickly induced, within 20-30 seconds, which is quite different from earlier thrombosis models, which required at least several minutes for occlusion.[3,4]

To confirm that the observed discoid platelet aggregation occurred on undisrupted ECs, we traced the endothelial layer by using fluorescent IB$_4$ isolectin and determined that the endothelium on which the thrombi developed was structurally intact (supplemental Figure 1); there was no extravasation of fluorescent dye (70-140 kDa fluorescent dextran; Figure 1B). By contrast, when we used small dextran (10 kDa), administration of recombinant TNF-α or IFN-γ led to visible extravasation of the fluorescent dyes, as previously reported, possibly reflecting the ECs' inflammation status (supplemental Figure 3).[24] Under normal conditions, however, we observed none of these phenomena, which indicates that the machinery involved in our model is quite different from that involved in earlier models that use high-power laser injury, often associated with EC disruption, exposure of the extracellular matrix, and increased vascular permeability.[27-29] How then is the formation of thrombus initiated in our model if exposed extracellular matrix is not involved? By using a fluorescent ROS indicator ([APF; 3'-(p-aminophenyl]) fluorescein), we confirmed that the trigger for platelet aggregation was ROS production after laser irradiation (specifically O$_2^-$) within all of the vessels examined (Figure 1C). In addition, we confirmed that an antioxidant and ROS scavenger, NAC, completely blocked the evoked platelet aggregation in vivo (supplemental Figure 4), suggesting the potential clinical usefulness of targeting ROS in the treatment of cardiovascular diseases.

Our visualization system also enabled characterization of the fibrinogen kinetics. When the injury was created by laser, patchy fibrinogen binding was observed after 20 seconds (Figure 1D). Then, after 10 minutes, we observed the solidification of the developing thrombus with fibrinogen/fibrin network formation, possibly achieved via the coagulation cascade (Figure 1E).

Proinflammatory TNF-α and IL-1 signaling in ECs contributes to the formation of thrombus

It has been suggested that inflammation and ROS play major roles in the pathogenesis of vascular and thrombotic diseases,[1,30] but a direct contribution of proinflammatory cytokines and ROS to thrombus formation has not been demonstrated. It is known, however, that under pathophysiologic conditions platelets can stick to an endothelial monolayer that is not disrupted or inflamed, without exposure of the extracellular matrix.[7,31,32] Normal resting endothelium has a nonadhesive surface, but activated and inflamed ECs treated with cytokines are known to promote the adherence of circulating blood platelets.

Therefore, to determine the contribution made by proinflammatory cytokine signaling to our thrombosis model, we first assessed the formation of thrombus by laser/ROS in KO mice deficient in the proinflammatory cytokine TNF-α or IL-1 (Figure 2). We found that initial adhesion of platelets to the vessel wall and subsequent thrombus growth were both markedly impaired in TNF-α KO mice (Figure 2D-F). We also observed similarly impaired thrombus formation in small arterioles (Figure 2B-C). When we calculated the initial platelet "attachment" and thrombus "development," we found that the impairment of thrombus formation in TNF-α and TNF-R1 KO mice was observed similarly all in small-sized capillaries (Figure 2), small-sized arterioles, and large-sized (femoral) arteries (supplemental Figure 5), indicating the usefulness as an evaluation method of thrombus formation in vivo in various sized
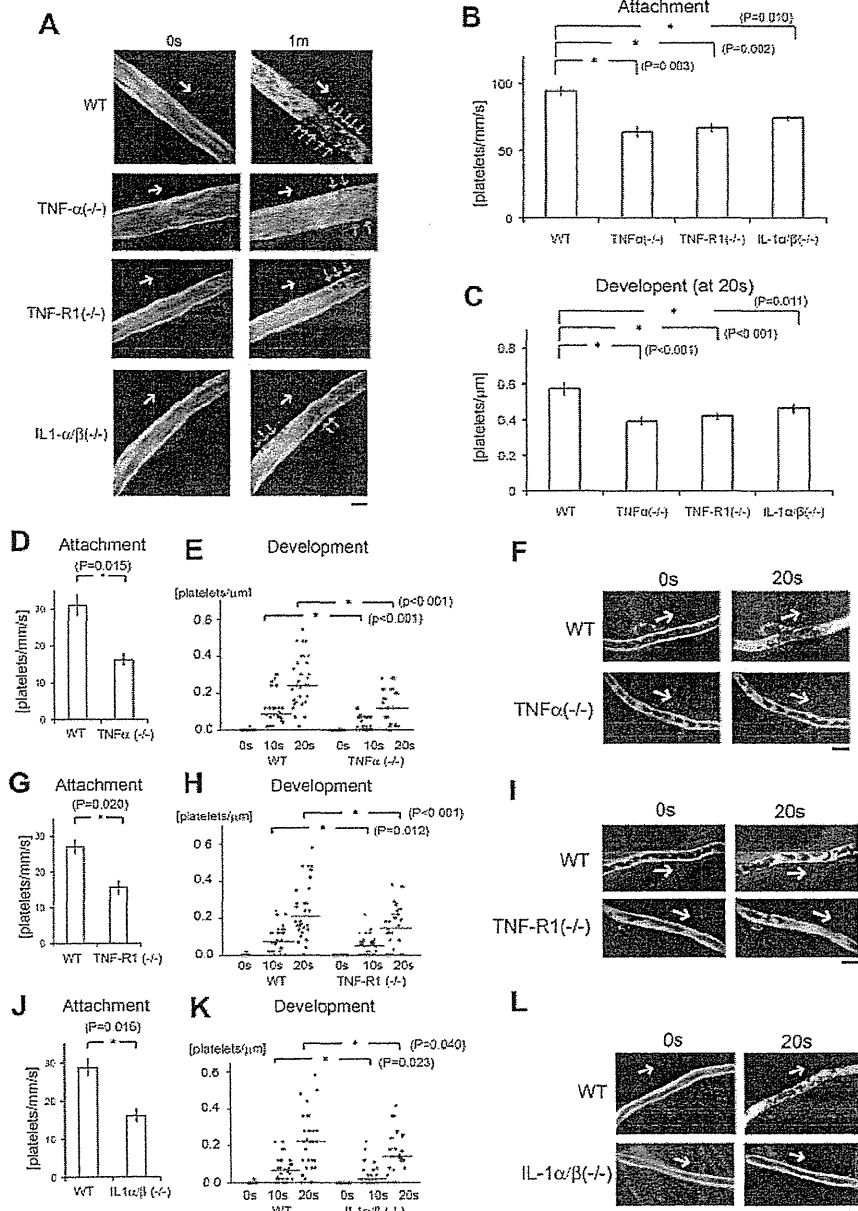
Figure 2. Inflammatory cytokines are key components for discoid platelet attachment and thrombus development in our laser/ROS-induced injury model. (A) In vivo imaging of thrombus formation in small-sized mesenteric arterioles of 12-week-old male TNF-α KO, TNF-R1 KO, and IL-1-α/β double KO mice and wild-type (WT) controls. The red arrows show the developing thrombi, and white arrows show the direction of blood flow. Numbers of platelets attached to the vessel wall 10 seconds after laser/ROS-induced injury (B) and numbers of platelets within the developing thrombus 20 seconds after injury (C) in each mouse type. The initial attachment of platelets to ECs after laser/ROS-induced injury was significantly diminished in all inflammatory cytokine KO mice, as was thrombus development. (D-L) Numbers of platelets attached to the vessel wall 10 seconds after laser/ROS-induced injury (D,G,J) and numbers of platelets within the developing thrombus 0 seconds, 10 seconds, and 20 seconds after injury (E,H,K) in mesenteric capillaries of 12-week-old male TNF-α (D-E) and TNF-R1 (G-H) KO mice, IL-1-α/β double KO mice (J-K), and their respective WT littermates. (F,I,L) In vivo imaging of thrombus formation within capillaries of TNF-α KO, TNF-R1 KO, and IL-1-α/β double KO mice and WT mice. The white arrows show the direction of blood flow. Both "attachment" and "development" were diminished in all inflammatory cytokine KO mice. Horizontal lines denote median values (E,H,K). (n = 30 vessels from 5 animals for each group). All scale bars are 10 μm.

vessels, and we can apply this thrombus formation technique also in femoral artery levels. We also confirmed the expression of TNF-R1 on the ECs of the mesenteric capillaries (supplemental Figure 6). Administration of rTNF-α restored impaired thrombus formation in TNF-α–deficient mice but not in TNF-R1–deficient mice, indicating that TNF-α is a key mediator possibly involved in ROS-induced thrombosis (Figure 3A-B).

We next examined how TNF-α/TNF-R1 signaling associated with ROS signaling can mediate the rapid formation of thrombus. To distinguish the role of TNF-α/TNF-R1 signaling in ECs from that in blood cells, we transplanted BM from TNF-α KO or TNF-R1 KO mice to generate chimeric recipient mice. The endothelium remained intact in the chimeras, but their blood cells were derived entirely from the transplanted BM. This approach previously enabled us to determine which cell type contributed to the impaired thrombus formation observed in the recipient mice (Figure 3C-D).[10] Notably, these chimeras exhibited no significant impairment of thrombus formation, which suggests TNF-α/TNF-R1 signaling in ECs, not blood cells, is critical for thrombus formation on undisrupted endothelium.

To further clarify how ROS trigger platelet aggregation, we performed a FACS analysis of ROS-treated ECs (Figure 4A-E). We found that laser-treated hematoporphyrin (O_2^-) markedly increased cell-surface expression of VWF in ECs and that this effect was completely blocked by the administration of NAC. This finding is consistent with an earlier report that O_2^-, but not H_2O_2, can directly induce VWF secretion from cultured ECs.[13] In HUVECs with si-RNA–mediated TNF-α knockdown, VWF mobilization was markedly reduced, indicating that TNF-α in ECs plays a key role in mobilizing VWF from the Weibel-Palade bodies to the cell surface on stimulation by ROS, mainly O_2^-. Moreover, the response to ROS stimulation was not diminished in platelets obtained from TNF-α KO or TNF-R1 KO mice, indicating that EC cells, not blood cells, are indispensible for the response to ROS/laser injury
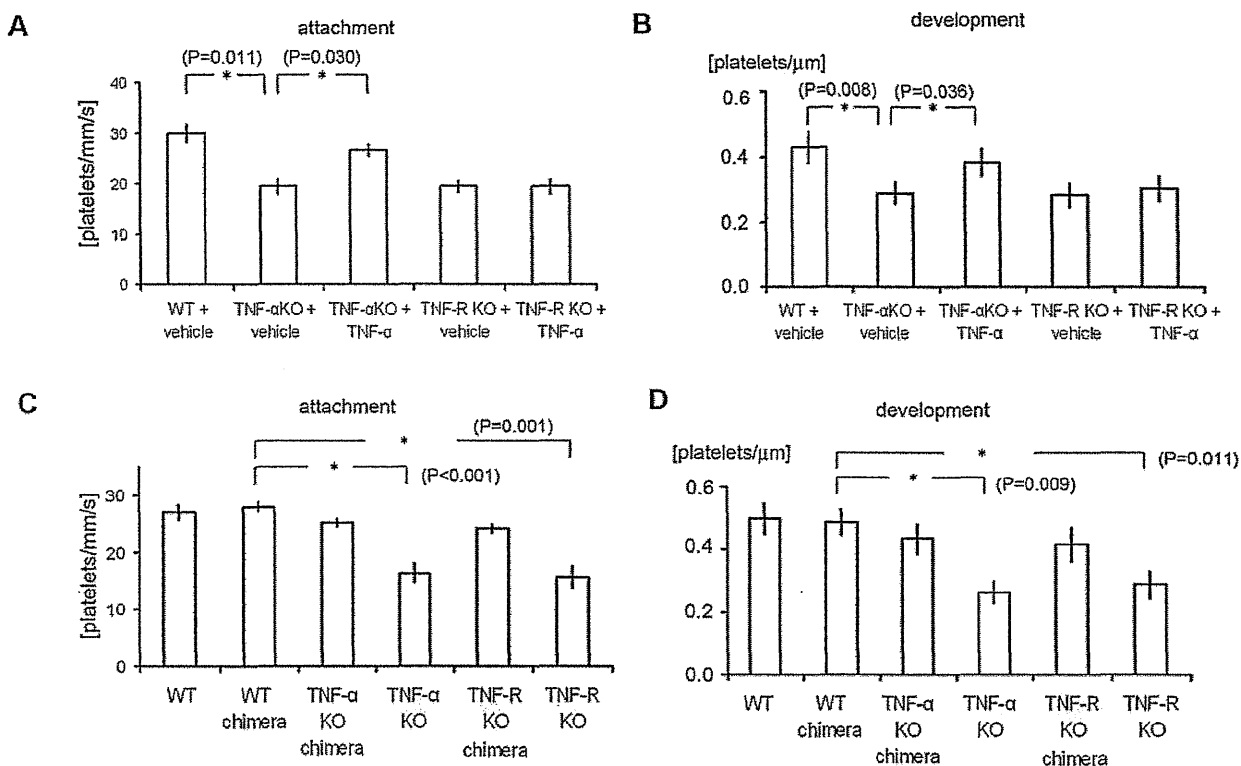
Figure 3. Analysis of TNF-α chimeric mice and the effects of TNF-α administration revealed the importance of inflammatory cytokine signaling in ECs in our thrombosis model. (A-B) Quantification of platelet attachment and thrombus development after laser/ROS-induced injury in 12-week-old male TNF-α and TNF-R1 KO mice and their wild-type (WT) mice treated with vehicle (PBS) or TNF-α (100 ng/kg; n = 30 vessels from 5 animals for each group). Recombinant TNF-α restored impaired thrombus formation in TNF-α–deficient mice but not in TNF-R1–deficient mice. (C-D) Platelet attachment and thrombus development after laser/ROS injury assessed in WT, WT-chimeric, TNF-α KO-chimeric, TNF-α KO, TNF-R1 KO-chimeric, and TNF-R1 KO mice. None of the chimeric mice showed impaired thrombus formation, in contrast to the total TNF-α KO and TNF-R1 KO mice, indicating that cell types other than blood cells contribute to thrombus formation in our model. Asterisks indicate statistical significance ($P < .05$).

in our model (Figure 4F-G). In addition, we confirmed that ROS increase endothelial P-selectin expression without affecting E-selectin expression (Figure 4A-B).

We also examined expression of the EC activation markers ICAM-1 and VCAM-1 after ROS stimulation of HUVECs to determine whether the impaired thrombus formation seen in TNF-α/TNF-R1 KO mice was simply caused by a lower degree of cell activation. Although hematoporphyrin (as a source of O_2^-) treatment for 20 minutes increased ICAM-1 and VCAM-1 expression slightly, si-RNA–mediated TNF-α or TNF-R1 knockdown had no affect (Figure 4C-D). In addition, short-term treatment (20 seconds, our stimulation time for thrombus formation) did not elicit these changes (data not shown). These results rule out the possibility that TNF-α deficiency reduced EC activation after treatment with ROS (O_2^-), leading to impaired thrombus formation in the KO mice. Considering that our thrombus model achieved very quick vessel occlusion in capillaries, EC and platelet activation after ROS treatment does not mainly contribute to our very quick thrombus formation in our new models.

Our in vivo results could be reproduced in vitro in microfluidic devices. We used a flow chamber system to assess in more detail how TNF-α/TNF-R1 signaling contributes to platelet attachment to cultured HUVECs (Figure 5). We found that administration of rTNF-α increased the attachment of platelets to HUVECs under high shear flow conditions (200 dynes/cm²), where platelet aggregation is dependent on the binding of endothelial VWF to platelet GPIbα.[33,34] si-RNA mediated knockdown of TNF-R1 on HUVECs reduced platelet attachment, again confirming that TNF-α/TNF-R1

signaling within ECs regulates platelet attachment to the endothelial surface under high shear conditions, which is consistent with our in vivo findings.

The results so far suggest that ROS (O_2^-)–dependent VWF mobilization is likely modulated via the TNF-α/TNF-R1 axis in ECs. To further test this idea, we analyzed endothelial VWF expression in vivo. Administration of Alexa 647-conjugated anti-VWF antibodies enabled visualization of the EC surface expression of VWF in vivo (Figure 6). Intravital staining revealed that after laser/ROS-induced injury, VWF appears on the surface of ECs within the affected capillaries and arterioles, which is consistent with our FACS results in ROS-treated HUVECs and with the idea that elevation of ROS levels induces the binding of VWF to GPIbα (Figures 4 and 6). Moreover, VWF intravital staining also indicated that mobilization of VWF after laser/ROS-induced injury was diminished in both TNFα KO and TNF-R1 KO mice, again confirming that TNF-α/TNF-R1 signaling participates in the rapid display of VWF on the EC surface (Figure 6 and supplemental Figure 7).

It is well recognized that platelets are important mediators involved in vascular inflammation, thrombosis, hemostasis, and atherogenesis,[7,35] and that inflammation is characterized by interactions between leukocytes, ECs, and platelets.[36] For example, activated platelets are known to produce IL-1α and -β.[2,37,38] Thus, determining the degree to which inflammatory cytokines are involved in platelet aggregation on ECs would further clarify the molecular link between thrombosis and inflammation.
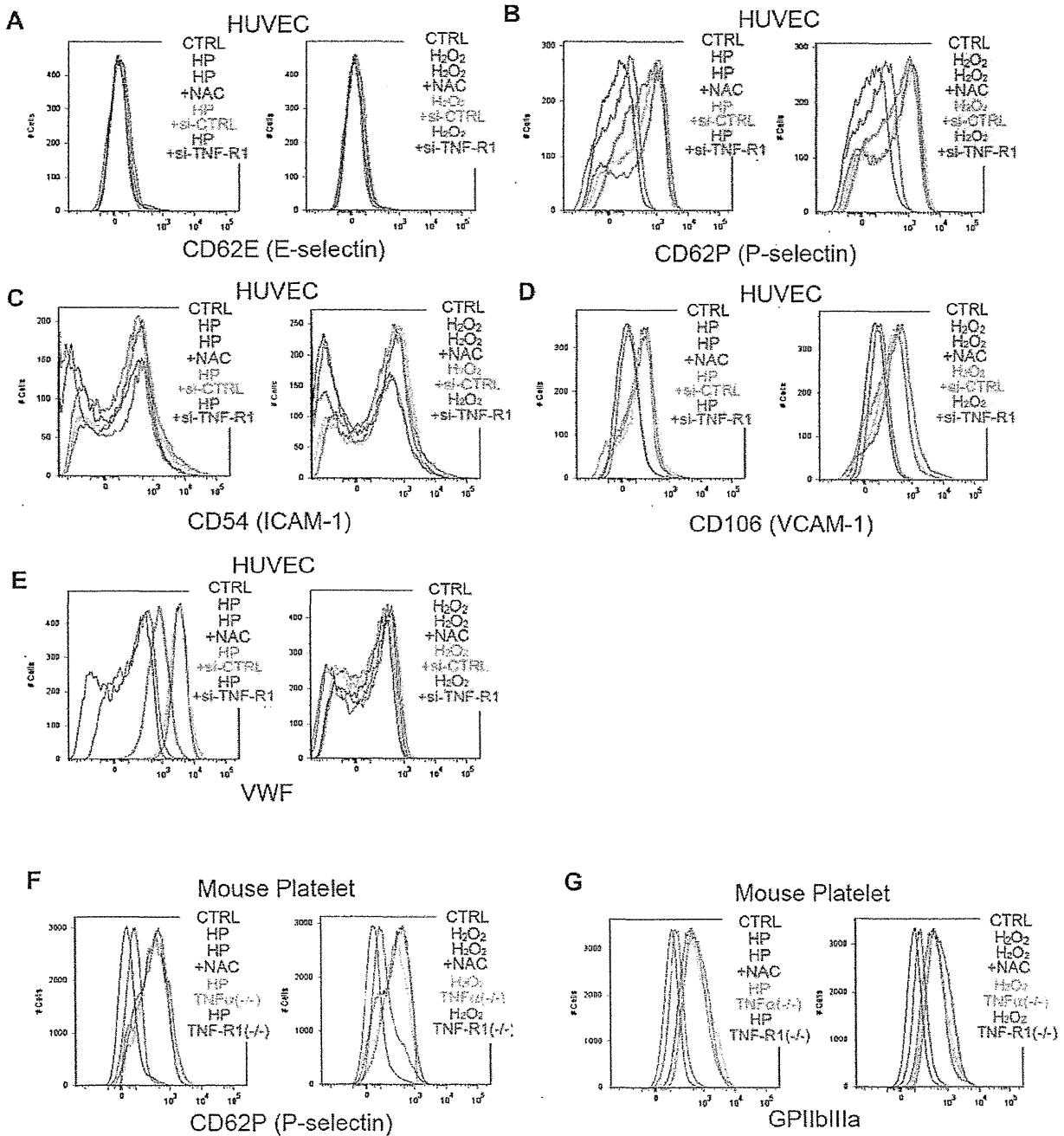
Figure 4. FACS analysis showing ROS-induced increases in VWF on HUVECs, and in P-selectin and GPIIbIIIa on mouse platelets. (A-E) Adhesion molecules, activation markers, and cell-surface VWF were analyzed by flow cytometry in cultured HUVECs. Some cells were treated with hematoporphyrin (1mM, HP, as a source of O_2^-) for 20 minutes and then stimulated with laser irradiation to induce ROS production. Other cells were treated with 1mM H_2O_2 and/or 100µM NAC for 20 minutes before the incubation with antibodies. Some HUVECs were treated with si-RNA targeting TNF-R1 (si-TNF-R1) or with control scrambled si-RNA (si-CTRL) 48 hours before the experiments. Black lines denote vehicle-treated control cells (CTRL); red lines, H_2O_2 or hematoporphyrin treatment; blue lines, ROS source plus NAC; green lines, si-CTRL and ROS; and purple lines, si-TNF-R1 and ROS. Note that O_2^- markedly increased cell surface expression of VWF on HUVECs, which was completely blocked by NAC, and diminished in si-TNF-R1 cells. Expression of P-selectin in ECs was also increased by ROS, without affecting E-selectin expression. ICAM-1 expression was moderately increased by O_2^-. (F-G) Washed platelets from 12-week-old male wild-type C57BL/6J, TNF-α KO and TNF-R1 KO mice were collected and analyzed after ROS stimulation as in the HUVEC experiments. Black lines denote vehicle-treated control cells from wild-type mice (CTRL); red lines, H_2O_2 or hematoporphyrin treatment; blue lines, ROS source plus NAC; green lines, ROS plus TNF-α KO platelets; and purple lines, ROS plus TNF-R1 KO platelets. Note that expression of P-selectin, and GPIIbIIIa was increased by ROS treatment, and that these effects were inhibited by NAC.

This prompted us to examine thrombosis in IL-1 α/β double KO mice (Figure 2J-L). We found that the initial adhesion of platelets to ECs after laser/ROS-induced injury was diminished in the double KO mice, as was thrombus growth, which indicates IL-1 signaling is also involved in ROS-mediated thrombus formation in our model. Conversely, we confirmed that both the initial attachment of platelets to the vessel wall and subsequent thrombus development are enhanced after laser/ROS-induced injury in IL-1 receptor antagonist KO mice (supplemental Figure 8). Thus, inflammatory processes associated with IL-1 production likely contribute to ROS-initiated thrombus formation.[35]
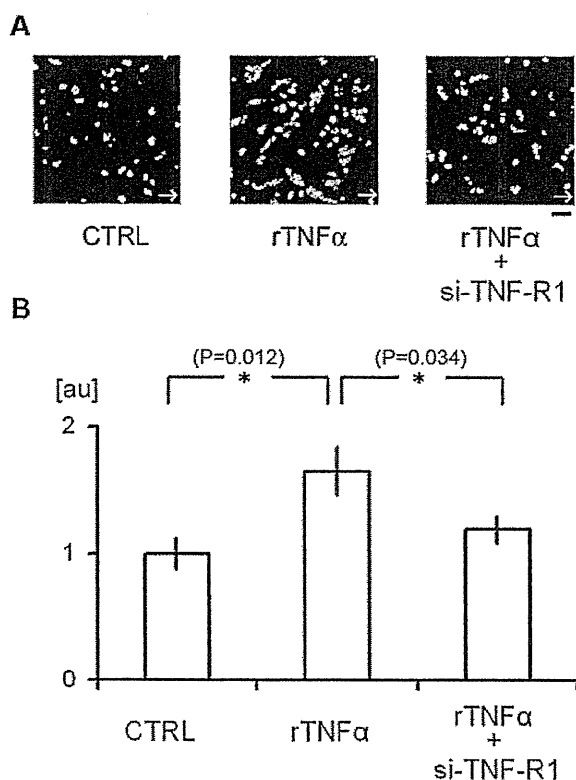
A

B

Figure 5. Flow chamber analysis of the contribution of TNF-α signaling to platelet attachment to HUVECs. (A-B) Attachment of human platelets to cultured HUVECs. Some cells were treated with si-TNF-R1 48 hours before the experiments; CTRL denotes HUVECs treated with control scrambled si-RNA. Some cells were also treated with human rTNF-α (24 hours, 10 ng/mL). After perfusing tetramethylrhodamine ethyl ester–stained platelets with Tyrode buffer for 5 minutes at 200 dynes/cm², adherent platelets were visualized (A). White arrows denote the direction of flow. The numbers of adherent platelets were quantified and normalized to the number obtained using CTRL cells (B). AU denotes arbitrary units. (n = 15 experiments for each group). Asterisks indicate statistical significance ($P < .05$). Scale bar is 10 μm.

Platelet activation agents induce formation of thrombi containing leukocytes and deformed platelets

To examine the formation of thrombi via mechanisms not involving ROS, we assessed the effect of promoting platelet aggregation in mice administered thrombin (supplemental Figure 9). Thrombin directly induces integrin-mediated inside-out signaling, leading to irreversible platelet aggregation.[39] After we administered thrombin, we observed formation of thrombi with a fibrinogen network (possibly fibrin) in occluded vessels. This effect was similar to the one seen in the long-term after laser/ROS-induced thrombus formation (Figure 1E). In contrast to the laser injury model, however, anti-GPIbβ staining showed that only 49.4% ± 7.0% of the cells (n = 30 occluded vessels) making up the thrombin-induced thrombi were platelets; the others were erythrocytes.al though leukocytes (14.5% ± 1.2%, n = 30 occluded vessels from 5 animals) were also present, suggesting platelet-leukocyte interactions play a major role in thrombin-induced thrombosis. However, the most remarkable finding was that the platelets within the thrombi had lost their discoid shape. Thus, the thrombosis that occurs in our model is quite different from that induced by platelet activating agents from the viewpoint of the cellular kinetics, and we consider our method to be a more useful tool with which to analyze single-platelet kinetics in the absence of other cell types, and to elucidate the effect of gene manipulation on single platelet function.

We also examined the effect of thrombin inhibitor (hirudin), and in vivo imaging showed thrombin inhibitor reduced the thrombus

development in late phase (20 seconds after laser injuries), but not the initial platelet attachment during first 10 seconds, indicating that thrombin contribute to the stabilization of developing thrombus in our models (supplemental Figure 10).

Integrin activation and thrombus stability

Initial platelet aggregation reportedly depends on a structural change in integrin αIIbβ3 (GPIIbIIIa) mediated by "inside-out" signaling through talin-binding at Leu746 and Tyr747 of the β3 integrin subunit.[14,15] In addition, evidence suggests the level of Tyr747 phosphorylation linked with the tyrosine phosphorylation of Fyn and Lnk may contribute to the stability of the developing thrombus in this model.[10] To test whether a selective deficiency on Tyr747 phosphorylation (Y747A knock-in [KI] mice) would influence laser/ROS-induced thrombus formation in vivo compared with a Leu746 deficiency (L746A KI mice), we repeated the thrombosis protocol by using these integrin mutant mice. in which talin-dependent integrin activation was eliminated (Figure 7).[15] After laser exposure, initial attachment to the vessel wall was unchanged in L746A KI mice (Figure 7A), but thrombus growth during the late phase was diminished (Figure 7B-C). However, both initial platelet attachment and subsequent thrombus growth were severely diminished in Y747A KI mice (Figure 7D-F), suggesting Tyr747 but not Leu746 is involved in initial platelet attachment leading to thrombus formation.

To evaluate the kinetics of thrombus growth and stability in more detail, we compared the changes in platelet number within developing thrombi in wild-type and Y747A mice (Figure 7G). In wild-type mice. the number of platelets within thrombi increased irreversibly. In Y747A KI mice, by contrast, platelet numbers within thrombi increased transiently but subsequently declined, reflecting the instability of the thrombi. It can be seen in Figure 7G. for example, that thrombi in Y747A KI mice were unstable and were washed away by the blood flow. From these findings, we conclude that talin-dependent integrin activation is required for thrombus stability and that phosphorylation at Tyr747 within the talin-binding NPXY motif of integrin is crucial.

Similar calculation of platelet numbers in developing thrombi showed that the platelet kinetics in TNF-α KO mice differed from both wild-type and Y747A KI mice (Figure 7G). Most notably, the initial attachment of platelets to the endothelium was delayed, which caused there to be a time lag before platelet numbers began to increase within thrombi. In addition, the subsequent accumulation of platelets was more gradual in TNF-α KO mice than in wild-type mice. The delayed initiation of thrombus formation in TNF-α KO mice may be caused by impaired adhesion of platelets to the undisrupted ECs, again suggesting TNF-α/TNF-R1 signaling contributes to VWF mobilization after ROS/laser injury.

To clarify the contribution made by platelet adhesion molecules in our thrombosis model, we again used flow cytometry to examine the effects of ROS stimulation on the expression of adhesion molecules on mouse platelets (Figure 4). We found that the levels of P-selectin and GPIIbIIIa expression on platelets were all increased by ROS treatment, and these effects were inhibited by NAC. However. the increase in the expression of these platelet activation markers was relatively mild compared with levels seen with platelet activation agonists.[40] Other markers of platelet functionality and activation were unaffected by ROS treatment. Again, the rapidity with which thrombi formed in our model (within 20 seconds) make it unlikely that ROS-induced EC or platelet activation is a primary contributor to thrombus formation in our new model.
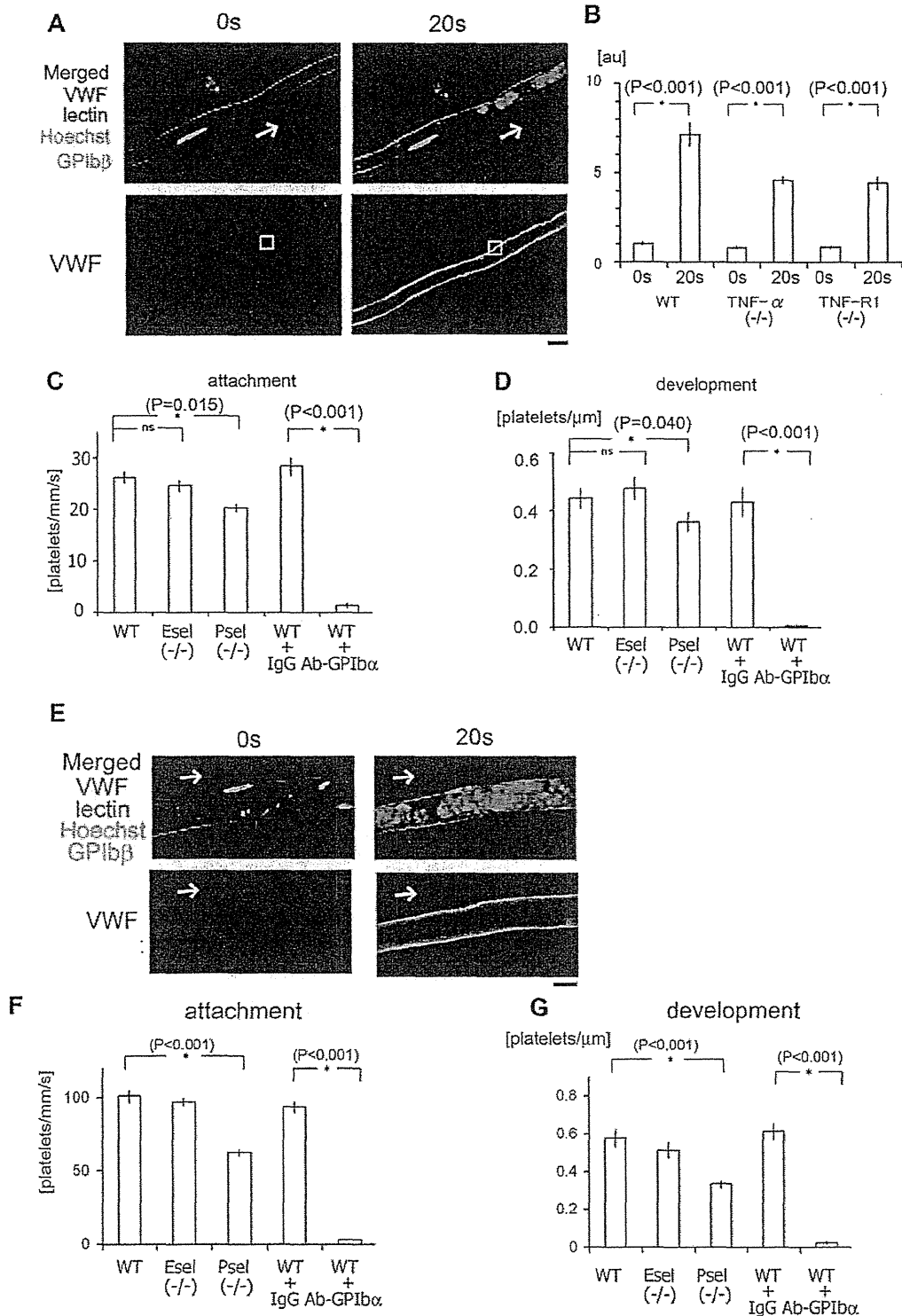
Figure 6. Binding of endothelial VWF to platelet GPIb plays a pivotal role in our laser/ROS-induced thrombosis model in both capillaries and arterioles. (A) In vivo imaging of VWF mobilization to the EC surface of small capillaries. Fluorescent anti-VWF antibody (red) was administrated to wild-type mice and visualized before and after laser/ROS-induced injury. VWF is expressed on the EC surface within the affected vessel after laser/ROS-induced injury. The cells were also costained with lectin (blue, vasculature), anti-GPIbβ (green, platelets), and Hoechst (green, nucleus). (B) Relative change in anti-VWF signals after laser/ROS-induced thrombus formation in wild type (WT), TNF-α KO, and TNF-R1 KO mice. Anti-VWF signal intensity was determined in the EC surface regions (white boxes in panel A) before (0 seconds) and 20 seconds after laser/ROS-induced injury. Note that VWF expression on endothelium after laser/ROS-induced injury was significantly reduced in both KO mice. AU denotes arbitrary units (n = 15 vessels from 5 animals). Representative original VWF images are shown in supplemental Figure 7. Asterisks indicate statistical significance ($P < .05$). (C) Numbers of platelets attached to vessel walls 10 seconds after laser/ROS-induced injury in WT, P-selectin KO (P-sel^{-/-}), and E-selectin KO (E-sel^{-/-}) mice, as well as WT mice treated with control IgG (WT + IgG), or neutralizing anti-GPIbα antibody (WT + Ab-GPIbα). Numbers of attached cells were markedly reduced in anti-GPIbα–treated WT mice (n = 30 vessels from 5 animals in each group). (D) Calculated numbers of platelets in developing thrombi 20 seconds after laser/ROS-induced injury (n = 30 vessels from 5 animals for each group). (E) Visualization of VWF mobilization to the EC surface in small arterioles, performed as in A. (F-G) Quantification of initial platelet attachment and thrombus development after laser injury in small arterioles (n = 30 vessels from 5 animals in each group). Asterisks indicate statistical significance ($P < .05$). The scale bar is 10 μm.

Actin cytoskeleton associated with lamellipodia formation is also required for thrombus stability

Because thrombus stability appeared to require a mechanical link between β3 integrin and the actin cytoskeleton, we next examined the role of actin cytoskeletal reorganization in our thrombosis model. Rac1 is the major mediator of lamellipodia formation in platelets in vitro.[16,17] In addition, Rac1 is reportedly required for thrombus stabilization in conventional in vivo thrombosis models entailing thrombin-stimulated actin reorganization,[16] and in thrombin-stimulated granule secretion.[41] When we assessed thrombus formation in platelet-specific Rac1 KO mice (platelet factor 4 promoter-dependent deletion of Rac1: Pf4-Rac1 KO), we found that only the late-phase thrombus stabilization was impaired, but the effect of Pf4-Rac1 KO was modest in comparison to Y747A KI (Figure 7D-F, and 7H-J). This finding indicates that both thrombin-PAR signaling-mediated integrin activation and Rac1 activation may be involved in thrombus stabilization, but not in initial platelet adhesion, and further confirm that tyrosine phosphorylation at Y747 of β3 integrin is likely required for stable adhesion of thrombi to the endothelium.

Binding of endothelial VWF to platelet GPIbα contributes to the initiation of discoid platelet aggregation

We next asked how ROS acting via the TNF-α/TNF-R1 axis cause ECs to trap circulating platelets, leading to discoid platelet aggregation in our models? We suspected that increased exposure of endothelial VWF might contribute to the binding of VWF to platelet GPIbα. To test that idea, we administered a neutralizing anti-GPIbα antibody, which completely blocked both platelet adhesion and thrombus development, which confirmed that that VWF-GPIb binding is a critical step in the rapid onset of discoid platelet aggregation in both capillaries and arterioles after ROS/laser injuries (Figure 6).

We also assessed the contributions of P-selectin and E-selectin to thrombus formation using respective KO mice. We found that P-selectin deficiency impaired both initial platelet adhesion and thrombus development, but the effect was relatively minor, compared with GPIbα inhibition. E-selectin deficiency did not alter thrombus formation (Figure 6).

From the results summarized in Figure 7G, which show that TNF-α deficiency delayed adhesion of platelets to ECs, we suggest that TNF-α/TNF-R1 signaling maintains and/or amplifies ROS signaling, leading to mobilization of VWF to the EC surface. Indeed, the absence of TNF-α/TNF-R1 signaling led to weak and delayed discoid platelet aggregation (Figures 2 and 7G). We therefore conclude that the rapid onset of discoid platelet aggregation on undisrupted ECs is mediated by proinflammatory cytokine signaling, even when the endothelium is not disrupted, and that subsequent thrombus stability is mediated via integrins and actin linkers. Finally, our in vivo imaging is not only useful for analyzing platelet kinetics, it could also provide novel clues to improved strategies for the treatment of thrombotic diseases.

Discussion

Severe vascular injuries cause de-endothelialization and exposure of the subendothelial matrix. However, it also has been reported that thrombosis can occur on the undisrupted endothelium.[7] It is therefore crucially important to determine how platelets and ECs interact to form thrombi in the absence of apparent disruption of the

vessel lumen. Our in vivo imaging system, which enables characterization of single-platelet kinetics during thrombus formation, revealed that (1) discoid platelet aggregation occurs rapidly on undisrupted endothelium after photochemical O_2^- production among mesenteric capillaries and arterioles and femoral arteries (Figure 1 and supplemental Figure 5); (2) the thrombi formed are composed almost entirely of discoid platelets (Figure 1 and supplemental Figure 2); (3) the proinflammatory TNF-α/TNF-R1 axis within ECs is a key regulator of this rapid attachment of platelets to the endothelium, possibly acting via stimulation of VWF display on the endothelium in response to ROS (Figure 2 and 7G); (4) the early phase of platelet attachment to undisrupted endothelium requires specific integrin signaling via Tyr747 but not Leu746 in the β3 cytoplasmic domain (Figure 7); (5) talin-dependent activation of αIIbβ3 integrin is indispensable for thrombus stability (Figure 7)[15]; (6) Rac1, which is essential for the actin reorganization needed for lamellipodial changes in vitro and thrombin-induced granule secretion, plays a major role in thrombus stabilization (Figure 7); (7) expression of P-selectin, but not E-selectin, is increased by ROS and contributes to platelet cohesion and subsequent thrombus development (Figure 6); and (8) the ROS scavenger NAC potently inhibits discoid platelet aggregation-based thrombus formation in our model, and also normalizes platelet activation after ROS treatment in vitro (Figure 4 and supplemental Figure 4).

With our system, we can visualize and quantitatively analyze single platelet kinetics in vessels ranging from capillaries to arterioles. Consequently, this method can be very effective for analyzing disease models targeting both small vessels (eg, disseminated intravascular coagulation) and larger arteries (eg, acute coronary syndrome closely related to thrombosis and artery occlusive diseases). Single-platelet analysis enabled us to separately examine the initial platelet attachment to vessels, thrombus growth, and stabilization of the developing thrombus, which are all dependent on different underlying molecular mechanisms. In addition, visualization of fluorescent molecules, such as fibrinogen and VWF, could be used to analyze the molecular kinetics in vivo, which would be useful for analyzing the cellular kinetics of thrombus formation.

In our model, thrombi were composed mainly of discoid platelets, without other cell types. By increasing the laser power and limiting the stimulation field to increase the ROS levels, we could induce platelet deformation like that seem after administration of platelet activation drugs such as thrombin (supplemental Figure 9 and 11), but the emergence of deformed platelets is a rare phenomenon. We therefore used moderate laser power to induce thrombus formation and mainly analyzed the kinetics of undeformed discoid platelets. This approach kept EC damage to a minimum and enabled us to address the clinical questions: How do platelets initially attach to vessel walls in living animals, and what are the first steps in the pathogenesis of cardiovascular diseases, especially those involving the occurrence of thrombotic events within vessels in the absence of plaque or erosion?[7]

Inflammation leads to an imbalance between the procoagulant and anticoagulant properties of ECs, which can lead to local stimulation of the coagulation cascade. TNF-α, the first proinflammatory cytokine released at sites of infection, is a potent inducer of immune defense mechanisms and a mediator of leukocyte recruitment. The authors of previous studies showed that TNF-α promotes coagulation by inhibiting synthesis of protein C and stimulating synthesis of tissue factor.[36] Here we observed impaired thrombus formation in TNF-α KO mice, and the results obtained with

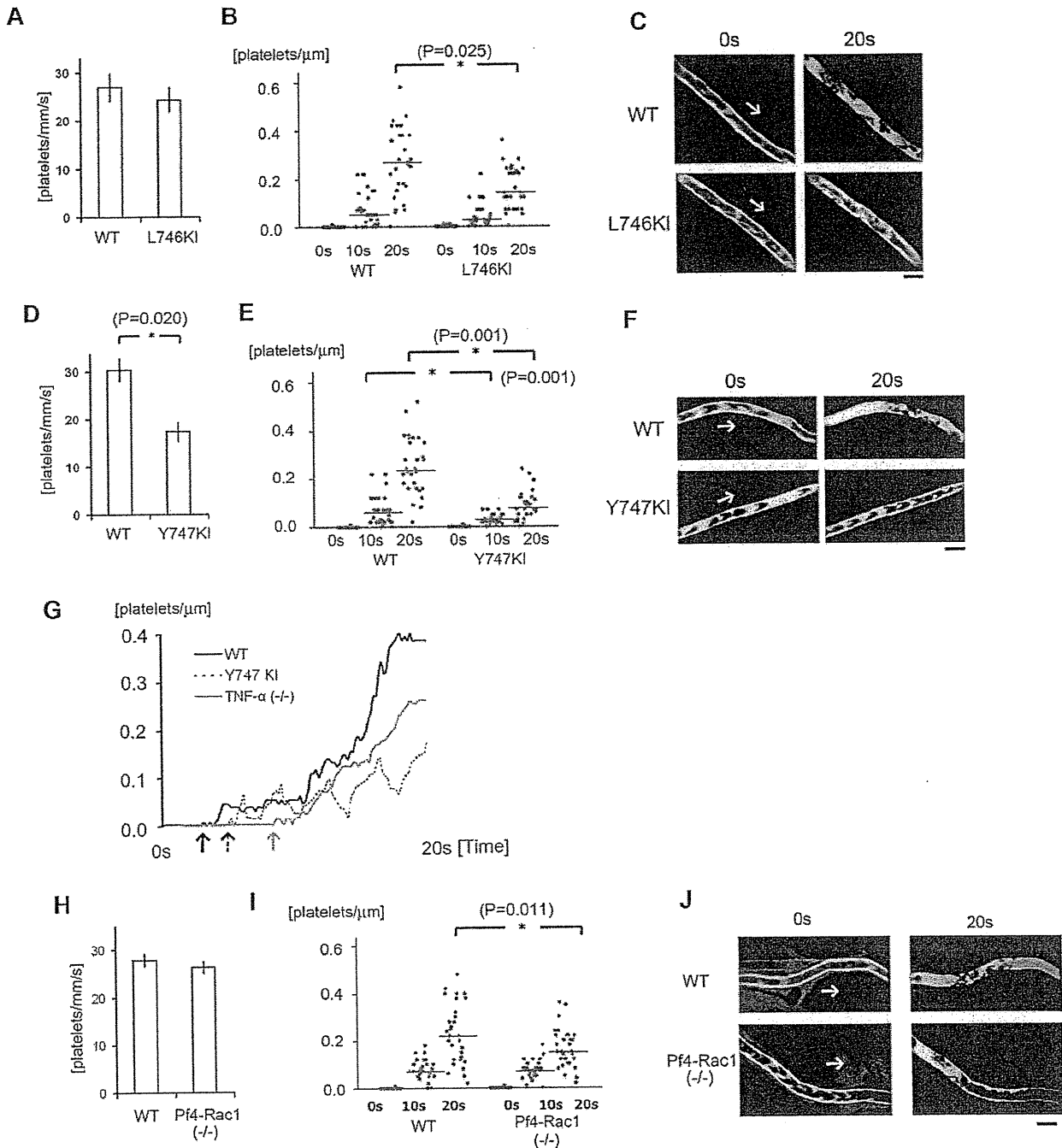**Figure 7. αIIbβ3 integrin signaling and actin cytoskeletal remodeling are required for stabilization of developing thrombi in vivo.** (A) Numbers of platelets attached to the vessel wall 10 seconds after laser/ROS-induced injury in L746A KI mice and their wild-type (WT) littermates (n = 30 vessels from 5 animals in each group). (B) Calculated numbers of platelets within developing thrombi 0 seconds, 10 seconds, and 20 seconds after laser/ROS-induced injury. (C) Representative in vivo imaging after laser injury (n = 30 vessels from 5 animals in each group). Scale bar is 10 μm. Asterisks indicate statistical significance ($P < .05$). (D-F) Thrombus formation in Y747A KI mice and their WT littermates. The experimental protocols were the same as in panels A-C. Note that thrombus formation is more severely impaired in Y747A KI mice than L746A KI mice. (G) Representative curve showing the numbers of platelets in a developing thrombus after laser/ROS-induced injury in wild-type (WT, black line), TNF-α KO (gray line), and Y747A KI (dotted line) mice. Arrows in each line show the time of initial platelet attachment to the endothelium. (H-J) Impaired thrombus formation in Pf4-Rac1 KO mice. Platelet attachment (H) and thrombus development (I) after laser/ROS-induced injury was quantified, and in vivo images are shown (J). Horizontal lines denote median values (B,E,I).

chimeric mice indicate that TNF-α/TNF-R1 signaling within ECs is a key positive regulator of thrombus formation. This is consistent with earlier results that ECs stimulated with inflammatory cytokines exhibit increased platelet adhesion.[42,43] We observed that ECs treated with TNF-α showed increased platelet attachment under flow conditions in vitro (Figure 5). Conversely, mobilization of VWF to EC surfaces after laser/ROS-induced injury was reduced

by TNF-α deficiency both in vivo and in vitro (Figure 6 and supplemental Figure 7), although the level of impairment of thrombus formation in TNF-α KO mice was not dramatic (Figure 2).

Considering that we were able to induce thrombus formation within seconds in capillaries after laser injuries, inflammatory cytokines within ECs, even at low levels, may determine sensitivities to ROS signaling and the levels of adhesion molecule

expression. In fact, VWF mobilization to the EC surface is, at least in part, mediated by TNF-α/TNFR1 signaling (Figure 6 and supplemental Figure 7). In addition, IL-1, which is present at relatively high concentrations in platelet granules, also appears to be involved in thrombus formation in our model. IL-1β has also been identified as a key mediator of platelet-induced activation of ECs,[44] and its production has been observed in activated platelets[2] (Figure 2). These findings, together with our observation that IL-1α and -β, play key roles in the initial attachment of discoid platelets to the vessel wall and in subsequent thrombus formation suggest a vicious cycle is activated in which thrombotic events stimulate pro-thrombotic inflammatory responses in both ECs and platelets.

ROS are key mediators of the signaling that underlies the vascular inflammation leading to atherogenesis.[9] Exogenous ROS reduce the threshold for platelet activation in response to agonists and induce spontaneous platelet aggregation through unknown mechanisms.[8] In addition, NAD(P)H-oxidase-dependent platelet ROS production enhances the recruitment of platelets to developing thrombi. It has been assumed that under pathophysiologic conditions up-regulation of O_2^- production by hyperactivated platelets serves as the physiologic basis for prolonged thrombus formation.[9] In addition, the oxidant stress linked to ROS production promotes dysregulation of ECs. All known risk factors for atherothrombosis promote ROS production,[8,45] and it is thus tempting to speculate that ROS and proinflammatory cytokines act in concert within the "inflamed" vasculature, although atherosclerotic lesions have not been directly visualized in human subjects. In the present study, we demonstrated that ROS rapidly induce the onset of thrombus formation on undisrupted endothelium independently of platelet agonists. In addition, platelet activation via talin-dependent αIIbβ3 integrin signaling appears to be critical for late phase thrombus stability in our model (Figure 7 and supplemental Figure 12).[46] Haling et al reported that talin-dependent integrin activation associated with actin cytoskeletal changes is required for fibrin clot retraction and is essential for thrombus stability.[47] Our in vivo findings are consistent with those earlier results.

We also found that the administration of NAC reduced levels of both GPIIbIIIa, as well as P-selectin expression in platelets, and inhibited platelet aggregation in vivo (Figure 4 and supplemental Figure 4). Although NAC is reported to be a potent inhibitor to plasma VWF multimers,[48] it may also act directly as a ROS scavenger, suggesting ROS scavenging might be a useful therapeutic strategy for inhibiting thrombus formation in vivo. Sarratt et al[49] reported that GPVI and integrin α2 play critical roles during platelet aggregation on collagen under flow conditions.

The present findings do not enable us conclude as to the precise molecular mechanism by which ROS acted via TNF-α signaling and VWF mobilization in ECs to induce thrombus formation. Whereas GPIbα blockade and NAC treatment almost completely blocked ROS/laser-induced thrombus formation in vivo (Figure 2 and supplemental Figure 4), TNF-α, TNF-R1, IL-1, and Rac-1 deficiency and functional integrin mutation all had only moderate effects on thrombus formation, though Y747A integrin mutation had a more marked effect. It may be that inflammatory cytokine and integrin signals act cooperatively with actin reorganization to mediate thrombus formation in our model. Alternatively, one or more as yet unknown factors might also influence VWF mobiliza-

tion. Although elucidating this mechanism could be important when considering possible future therapeutic interventions, we considered that this is beyond the scope of this technical report.

In summary, by using our imaging system, we have clarified the mechanism by which thrombi are rapidly formed by discoid platelets on undisputed endothelium. Specifically, in vivo imaging along with kinetic studies showed the importance of endothelial TNF-α and IL-1 signaling for initiating GPIb binding to VWF. The initial platelet aggregation subsequently leads to irreversible integrin- and actin-dependent thrombus development.

Jackson et al's previous findings show that shear gradient induced the discoid platelet aggregations,[5,6] and here in we clarified that inflammatory cytokine signaling in ECs play pivotal role in discoid platelet aggregations in vivo. Although, they did not claim the specific molecular mechanisms, but it is tempting to speculate that shear gradient changes and inflammatory cytokine signaling coordinately contribute to the discoid platelet aggregations leading to the vessel occlusion.

Authorship

Contribution: S.N., M.N., S.K., Y.I., N.T., J.O., M.O., A.K., B.P., T.U., T.K., S. Sato, and A.A. performed experiments; S.N., I.M., and K.E. analyzed results and made the figures; and S.N., I.M., B.P., H.Y., S. Sugiura, T.K., H.N., K.E., and R.N. designed the research and wrote the paper.

Conflict-of-interest disclosure: The authors declare that no competing financial interests.

Correspondence: Satoshi Nishimura, MD, PhD, Department of Cardiovascular Medicine, The University of Tokyo, 7-3-1 Hongo, Bunkyo-ku, Tokyo 113-8655, Japan; e-mail: snishi-tky@umin.ac.jp; and Koji Eto, MD, PhD, Clinical Application Section, Center for iPS Cell Research and Application, Kyoto University, 53 Shogoin-Kawaharamachi, Sakyo-ku, Kyoto 606-8507, Japan; e-mail: kojieto@cira.kyoto-u.ac.jp.